Examination of Vortex Deformation During Blade–Vortex Interaction

M. B. Horner,* R. A. McD. Galbraith,† and F. N. Coton‡
University of Glasgow, Glasgow G12 8QQ, Scotland, United Kingdom
and
J. N. Stewart§ and I. Grant¶
Heriot–Watt University, Edinburgh EH14 4AS, Scotland, United Kingdom

Results of a blade–vortex interaction (BVI) study incorporating particle image velocimetry (PIV) are presented. Test cases encompass a variety of intersection geometries, including head-on parallel interactions. Results provide quantified flow visualization images of the flows generated during interactions. The deformation and division of the interaction vortex during head-on interactions are documented. In addition, secondary vortical structures generated during interactions are observed and their effect upon the interaction vortex is examined. All PIV results are examined in the light of understanding gained from previous pressure measurements made from the same BVI facility.

Nomenclature

C_{mQC} = quarter-chord moment coefficient
C_n = normal force coefficient
C_t = tangential force coefficient
c = blade chord length
R = blade radius
r = radial position of pressure measurement pod
X_v = horizontal distance between the leading edge, at the measurement position, and the vortex center, measured perpendicular to the vortex core
Y_v = vertical displacement of the vortex generator junction above the rotor disk
Z_v = lateral displacement of the vortex generator from the tunnel centerline
δ = vortex generator section incidence
Γ_c = vortex core circulation
Ψ = blade azimuth angle

Introduction

U NDER certain conditions of powered descent or vigorous maneuvering, rotorcraft blades pass through the wake and trailed tip vortices from previous blades (see Fig. 1). This interaction of the rotor blade with the tip vortex of a preceding blade has been identified as a significant source of noise and vibration in rotorcraft.[1-3] The need to reduce these undesirable effects requires the rotorcraft designer to have a clear understanding of the fluid dynamics underlying the phenomenon of blade–vortex interaction (BVI). This need has been addressed through both experimental[4-32] and computational[33-36] studies attempting to isolate the BVI from the rotor environment.

In pioneering wind-tunnel studies at the University of Pennsylvania, Surendraiah[4] and, subsequently, Padakannaya[5] utilized an upstream wing tip to generate a vortex that interacted with a downstream rotor. These studies were able to document many of the gross features of the BVI, including the development and collapse of a

large leading-edge suction peak and the associated buildup and reversal of the normal force. In studies[6-8] using a similar experimental technique, researchers working at NASA Ames were able to generate pressure data with better chordwise resolution than attained by Surendraiah[4] and Padakannaya.[5] In addition to the gross features of the interactions that had been previously identified, these researchers were able to document a convective disturbance in the aerofoil pressure distribution associated with the overhead passage of the interaction vortex. Unfortunately, neither the study from the University of Pennsylvania nor the studies conducted at NASA Ames were able to provide flowfield information, and therefore many of the important inferences associated with flowfield behavior remained unsubstantiated.

Pertinent flowfield information has been provided from a series of low-speed BVI tests, but utilizing a different experimental configuration. In these studies an interaction is produced by placing a two-dimensional aerofoil in the wake of a device that sheds (spanwise) vorticity. In one of these studies, Ziada and Rockwell[31] exploited both hydrogen bubble and dye injection methods to document the impingement of a series of vortices upon the leading edge of a wedge. These vortices were continuously produced by the destabilization of a shear layer a suitable distance upstream of the wedge. They observed and documented the convective trajectory of these vortices and also the formation of secondary vortices shed from the leading edge. Although many interesting facets of the flowfield behavior were described, its significance to rotor applications is limited by the extremely low Reynolds number, the lack of a trailing edge to the blade, and by the influence of other vortex elements upon the blade during interaction.

A similar experiment was reported by Booth and Yu.[26] In this study an oscillating upstream aerofoil produced a continuous series of vortices that convected over a trailing aerofoil. The work provided an insight into vortex convective behavior, but the quality of the
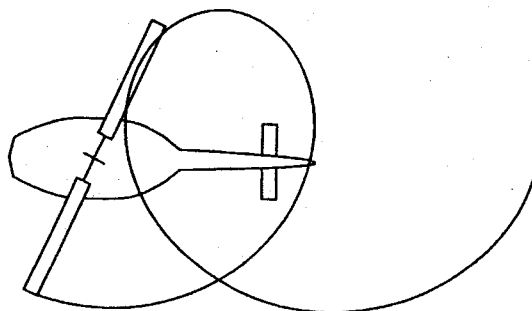
*Research Assistant, Department of Aerospace Engineering; currently Researcher, Bioserve Space Technologies, University of Colorado, Boulder, CO 80309.
†Head, Department of Aerospace Engineering.
‡Lecturer, Department of Aerospace Engineering.
§Research Assistant, Department of Civil and Offshore Engineering; currently Research Fellow, Department of Aeronautics, Imperial College, London SW7 2BX, England, United Kingdom.
¶Professor, Department of Civil and Offshore Engineering.

Fig. 1 Rotorcraft experiencing BVI.

smoke flow limited the amount of additional information available. Like the work of Ziada and Rockwell,[31] Booth and Yu[26] were unable to isolate a single interaction because of the vortex generator method. The experiments of Walker,[32] however, did isolate single BVIs at Reynolds numbers as high as 2×10^5 by a ramp and hold motion of the upstream aerofoil rather than the prior oscillating method. In the resulting interaction, strong vortex shedding from the trailed blade was evident, in addition to other flowfield features. Unfortunately, this study was primarily directed at canard–wing interactions and not those of helicopter rotors. All of their interactions reflected the influence of both the interaction vortex and the very large positive incidence produced by the upwash of the vortex generator itself.
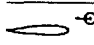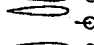
The present study is the second phase of a program being conducted at Glasgow University to isolate and examine the phenomenon of BVI. Subsequent phases will involve an examination of the effect of blade lift and the potential for BVI moderation through the generation of alternate tip vortex structures. In the current phase, the effects of the overhead passage of the vortex were examined in an experimental setup similar to that developed by Surendraiah. An upstream vortex generator produces a vortex that interacts with a downstream rotor. Flow visualization information and velocimetry data were obtained during interactions through the use of particle image velocimetry. These data were obtained under the same conditions used in previous studies conducted in the BVI facility at the University of Glasgow in which surface pressure data were recorded.[9-21] This allows a direct comparison of the two data sets and for validation of the flow inferences made from the surface pressure measurements.

Methods

Experiments were conducted in the University of Glasgow Handley Page wind tunnel in collaboration with the particle image velocimetry (PIV) facilities of Heriot–Watt University. An untwisted, nonlifting, single blade rotor interacted in a parallel or oblique manner with an oncoming vortex generated upstream of the rotor disk by a stationary wing. PIV was used to document flows about the rotor blade during interactions. The experimental setup is illustrated in Fig. 2.

The aluminium rotor blade had a NACA 0015 aerofoil section, with a 0.149-m chord and a 0.9426-m radius. The vortex generator was composed of two adjoining NACA 0015 aerofoil sections spanning the height of the test section 2.1 rotor radii upstream of the rotor hub. During the test sequence conducted in the 1.61×2.13-m octagonal test section, the tunnel speed was 47.0 m/s, whereas that of the rotor tip was 59.25 m/s. The vortex strength was controlled by setting the two sections of the vortex generator at equal but opposite incidence. The horizontal position of the vortex generator (Z_v) was altered to control the angle of intersection between the interaction vortex and the blade, resulting in either a nominally parallel or oblique BVI. The vertical position of the aerofoil junction on the vortex generator (Y_v) was varied to allow an examination of interactions for different blade–vortex separation heights. PIV data were

Fig. 2 Experimental setup in the University of Glasgow Handley Page wind tunnel.

Table 1 Case matrix of PIV tests run in the Glasgow University BVI facility

| Aerofoil/vortex geometry	Test case	Y_v/c	Γ	Z_v/c	r/R
	P7511	0.2	6.7	0.0	0.78
	P7502	0.1	6.7	0.0	0.78
	P7501	0.0	6.7	0.0	0.78
	P7491	−0.2	6.7	0.0	0.78
	P7391 (weaker vortex)	0.0	6.7	0.0	0.78
	B7511 (2nd quadrant oblique)	0.2	6.7	−1.0	0.78
	Y7511 (3rd quadrant oblique)	0.2	6.7	−1.0	0.78
	P9511 (near the blade tip)	0.2	6.7	0.0	0.94
	P9491 (near the blade tip)	−0.2	6.7	0.0	0.94

collected in one of two planes oriented perpendicularly to the tunnel freestream, one plane at 0.78 rotor radii upstream of the rotor hub and the second at 0.94 rotor radii.

Flows were examined in nine different combinations of interaction geometry and measurement position, thus allowing a comparison of data collected during parallel and oblique interactions, near the tip, inboard, and for several different interaction heights. The full test matrix is presented in Table 1.

PIV data were collected in the measurement plane by photographing Expancel DE20 mircoballoon seeding particles illuminated by a pulsed sheet of laser light. These particles have an average diameter of 20 μs and an average specific gravity of 0.06. To minimize flowfield disturbances, an upstream-facing 35-mm camera (Nikon F801) was mounted five chord lengths downstream of the measurement plane below the rotor hub. Images were collected on Kodak Recording Film 2475 using a 55-mm flat field lens. The camera mount was constructed of 49-mm box section mild steel, attached directly to the floor of the wind-tunnel bay, thus isolated from the vibration of the tunnel and rotor system. A faring covering the camera mount and the lower half of the rotor shaft was also employed to shield the camera mount from any aerodynamic buffeting. An accelerometer attached to the top of the camera mount indicated that errors in velocity measurement caused by camera vibration were less than 0.3% of the maximum velocities recorded in the measurement plane. The laser light required was provided by a Lumonics HLS4 ruby laser. The laser beam was formed into a light sheet using a simple lens configuration. Triple pulses of laser light were used to generate multiple images of each seed particle on the photographic film, thus allowing later calculation of local velocities in the vicinity of each particle. Laser pulses were typically separated by 50–100 ms, with each individual pulse having an energy of approximately 1.5 J. Directional ambiguity was addressed in a select number of tests by setting the first interpulse interval longer than the second. This procedure resulted in unequally spaced three spot patterns that can be used to derive flow direction. Most tests, however, utilized constant interpulse intervals of 60–80 ms.

Image processing was carried out in the Fluid Loading and Instrumentation Centre in the Department of Offshore and Civil Engineering at Heriot–Watt University in Edinburgh. During image processing the negatives are mounted on an X-Y traverser and interrogated using a charge-coupled device camera and microscope lens arrangement (see Fig. 3). Each 35-mm negative is subdivided into 80 frames (512×512 pixels) that are individually digitized. Computer software is then employed to automatically identify particle pairs or triples and to determine local velocity. A manual check is required for the rejection of spurious velocity vectors. For further information on the image processing technique see Liu.[37]

Image processing of each data negative requires approximately 1–2 h. As a result conventional data averaging is excessively time consuming and was not used. Instead, to obtain a representative
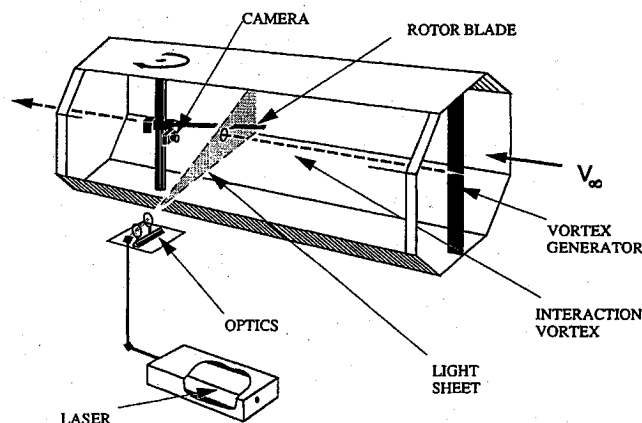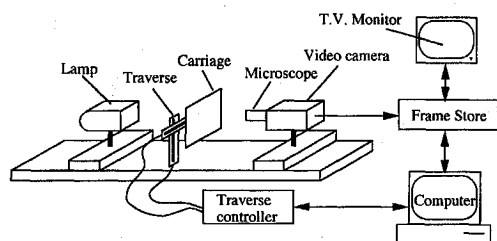
Fig. 3 Image processing facility at Heriot–Watt University.

image for each test condition, 12 or more images were recorded at each azimuthal position, and then the relative positions of the blade and vortex in each of the twelve images were determined. A judicial selection was then made and the chosen frame processed. Under some conditions the interaction vortex passes above the aerofoil and so out of the camera's view. In these cases a second camera, mounted above the rotor hub, and operating simultaneously with the lower camera, was used. Data from the upper camera simply documented the overhead position of the vortex as an aid in selecting the lower camera image representative of flows beneath the blade. The upper camera was not used for collecting velocimetry data.

Results

Flowfield velocimetry data were collected about the aerofoil during interaction with a free vortex These data documented many of the flow features observed in the previous studies discussed earlier. In addition, however, the velocimetry data quantified the spatial flow direction and magnitude, providing a quantified assessment of the temporal flow development.

Typical raw PIV data are presented in Fig. 4. This image captures the motion of the seeding particles during a head-on parallel interaction. Only a select portion of the original data negative is presented to allow better magnification of the particle images near the interaction vortex. The seed particles and the rotor blade have been illuminated by a triple pulse of the laser sheet, resulting in a triple exposure of the blade and of each particle. The aft portion of the aerofoil is evident as a brightly lit edge at the bottom of the figure. A close examination of this image will also reveal the motion of the seed particles as indicated by the displacements of their successive exposures.

Reduced data, in the form of a velocity vector map, are presented in Figs. 5a–5h. The tail of each vector in these figures indicates the measurement location, and the length and directional orientation are representative of the velocity magnitude and direction, respectively. These data do not include the velocity component associated with blade movement. The spatial scales are in millimeters, with the origin positioned at the aerofoil leading edge. The obvious dearth of data in the vortex core in each of these figures is simply a consequence of the gradual evacuation of the seeding particles as a result of the strong radial accelerations. Typical circumferential velocities of the vortex range from 25 m/s close to the core down to 6 m/s in the near field.

Figures 5a–5h present data from a head-on parallel interaction ($Y_v/c = 0.0$ and $Z_v/c = 0.0$). In Fig. 5a, the data capture the flowfield at an azimuth of 169 deg, with the vortex half a chord length in front of the leading edge. The strong vortex-induced upwash combined with the aerofoil motion result in an incidence of 18 deg. The flow above the upper surface has a characteristic arched appearance evident above the suction surface (upper or lower) in all tests. Although one does expect to see more flow curvature (local vorticity) above the suction surface, the presence of this curvature can also be interpreted as the effect of the blade in displacing fluid. Fluid near the leading edge is necessarily deflected away by the advancing blade, and fluid near aft portions moves back to fill space evacuated by the blade. In Fig. 5b the rotor has reached the 171-deg azimuth. In this figure the blade has reached a position only a third of a chord from the vortex center. The vortex upwash is even stronger here, and the incidence at the leading edge (including the aerofoil motion) has reached 31 deg.

In Fig. 5c the rotor has reached an azimuth of 174 deg. At this point the blade has penetrated through to the inner portions of the
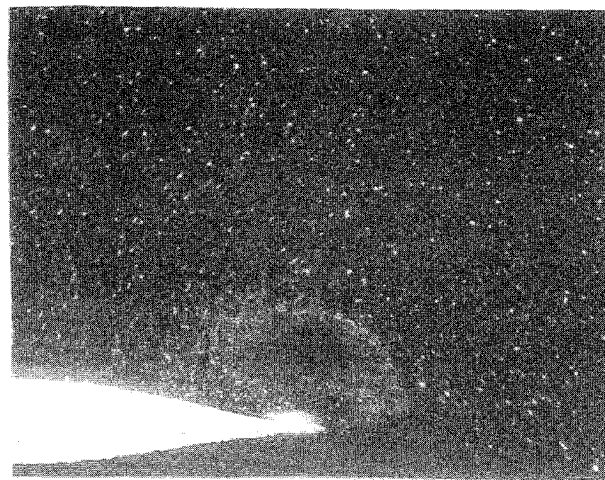

Fig. 4 Typical raw data collected during a BVI; $Y_v/c = 0.0$, $Z_v/c = 0.0$, $\Gamma_c = 3.4$ m²/s, and $\Psi = 184$ deg.

vortex core. This intrusion has resulted in the beginnings of a separation of the vortex into two fragments. On the lower surface the vortex fragment remains clearly defined as it maintains a rolled-up appearance. On the upper surface this definition is less clear because of a lack of data vectors near the blade surface. The strong vertical component of the fluid velocities in regions just aft of the upper vortex fragment and the tight arch to flows further aft are indicative of a particularly strong concentration of upper surface vorticity generated by the approach of the interaction vortex.

In the next frame (Fig. 5d) as the blade passes 180 deg, the two vortex fragments are beginning to exhibit substantially different convective behaviors. The upper vortex fragment has reached a position two-thirds of the way back along the blade surface, whereas the lower fragment has not yet reached the mid chord. Clockwise vorticity below the blade extends from the leading edge to the trailing edge. In contrast, on the upper surface vorticity remains closer to the vortex fragment, with regions of the flow above the leading edge exhibiting a slight anticlockwise curvature, indicating small concentrations of vorticity of opposite sense from the interaction vortex, and highlighting the narrow bounds of clockwise vorticity on this surface. Aft of the upper vortex fragment, there is a scarcity of velocity vectors near the blade; nevertheless, those vectors that are present indicate flow curvature produced by a local concentration of counterclockwise vorticity. Although it is not clear whether this vorticity has in fact rolled up to produce a discrete vortex, this vorticity has been christened the trailing-edge vortex. This trailing-edge vortex is similar to that seen in overhead interactions (see Ref. 21). At this point in the interaction the wake first comes into view, and no organized sense of shear is evident.

In Fig. 5e the data characterize flows as the blade reaches an azimuth of 182 deg. In these data the trends noted in Fig. 5d are more evident: vorticity on the lower surface is more distributed across the chord and slower in convection than on the upper surface. The collection of secondary vorticity christened the trailing-edge vortex is becoming more clearly defined in this image, revealed in a region of tightly circulating flow immediately above the blade trailing edge and aft of the large interaction vortex fragment. This trailing-edge vortex appears to be moving into a position between the interaction vortex and the trailing edge. This is the same vortex convective behavior noted in overhead interactions (see Ref. 21). Shears in the wake exhibit a weak clockwise sense. These trends are again evident in Fig. 5f, presenting data collected at an azimuth of 184 deg. This figure is particularly clear in documenting the trailing edge vortex as it convects past the trailing edge.

In Fig. 5g, the blade has reached an azimuth of 186 deg. In this figure the continued strong downwash induced by the interaction vortex fragments results in an incidence of −13 deg. The difference in convection properties of the two fragments has resulted in the upper surface fragment convecting entirely into the wake; however, on the lower surface vorticity still remains spread across the entire
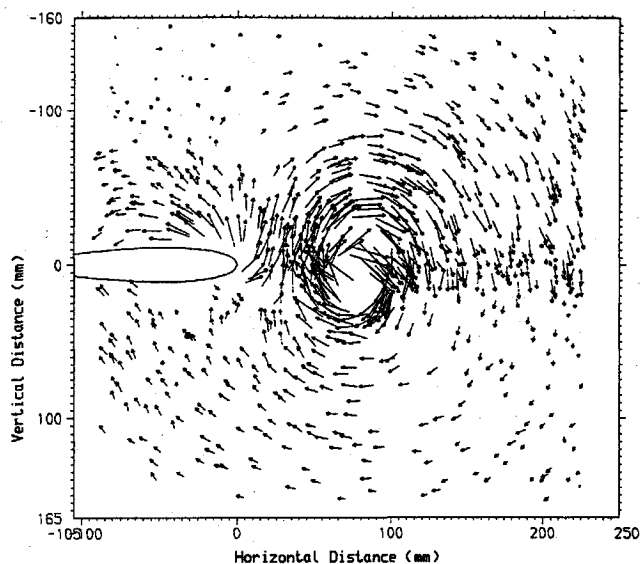
Fig. 5a PIV data collected during a parallel, head-on, BVI; $\Gamma_c = 3.4$ m^2/s, $r/R = 0.78$, $Y_v/c = 0.0$, and $\Psi = 169$ deg: →, 10 m/s; →, 20 m/s; and ——→, 30 m/s.

Fig. 5c PIV data collected during a parallel, head-on, BVI; $\Gamma_c = 3.4$ m^2/s, $r/R = 0.78$, $Y_v/c = 0.0$, and $\Psi = 174$ deg: →, 10 m/s; →, 20 m/s; and ——→, 30 m/s.
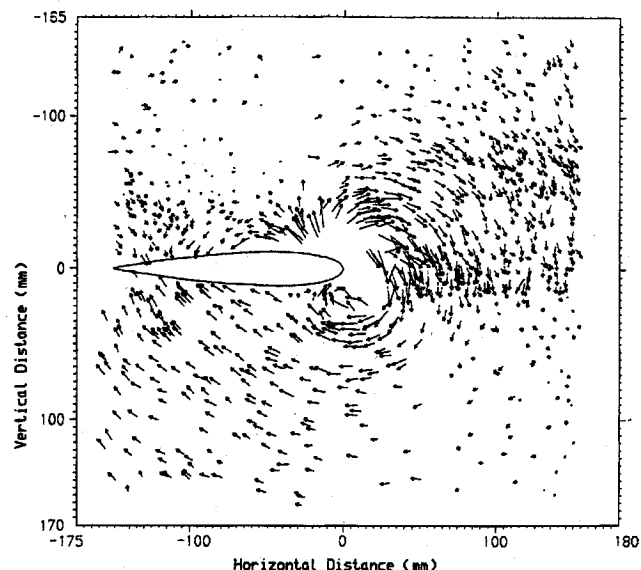

Fig. 5b PIV data collected during a parallel, head-on, BVI; $\Gamma_c = 3.4$ m^2/s, $r/R = 0.78$, $Y_v/c = 0.0$, and $\Psi = 171$ deg: →, 10 m/s; →, 20 m/s; and ——→, 30 m/s.
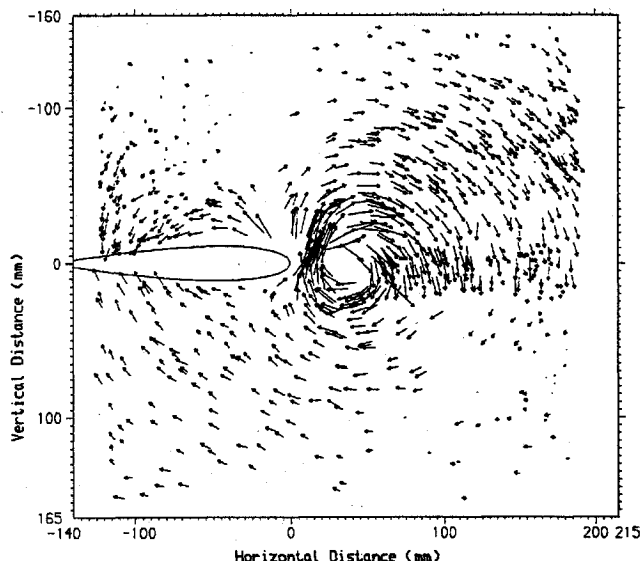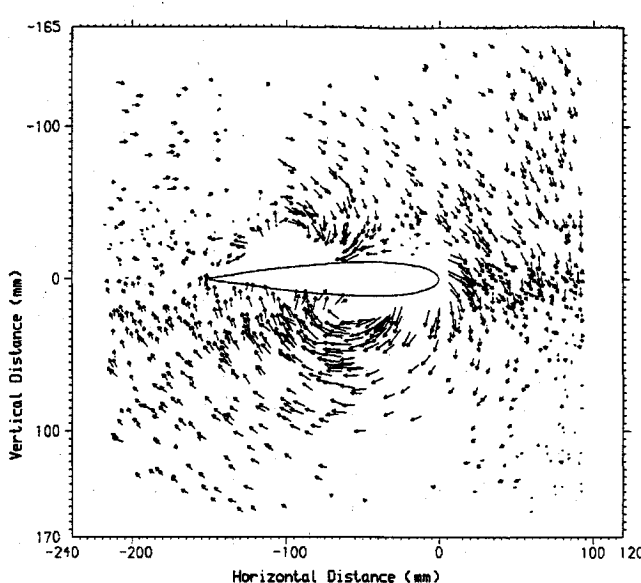

Fig. 5d PIV data collected during a parallel, head-on, BVI; $\Gamma_c = 3.4$ m^2/s, $r/R = 0.78$, $Y_v/c = 0.0$, and $\Psi = 180$ deg: →, 10 m/s; →, 20 m/s; and ——→, 30 m/s.

chord. The strongest regions of flow curvature, presumably marking the center of the vorticity in the lower fragment, are only just reaching the trailing edge at this azimuth. At this point, shear in the far wake shows a clockwise sense, whereas shear near the trailing edge shows the opposite sense.

Finally in Fig. 5h, as the blade passes 191 deg, the lower surface vortex fragment is seen in the wake. Although there is some confusion in the orientation of vectors between the lower vortex fragment and the trailing edge, it appears that the trailing-edge interaction has generated a small secondary vortex with an anticlockwise sense positioned between the lower vortex fragment and the trailing edge. This lower surface trailing-edge vortex is similar to one observed trailing behind the main interaction vortex in lower surface interactions (see Refs. 20 and 21). A third area of vorticity is apparent near the coordinates (−320, 40). Similar vortical structures are evident in many PIV data images collected in the later portions of all interactions, and these vortices typically appear to drift towards the right with increasing azimuth. Two possible explanations for the presence of these structures may be the associated tip vortex or shed vorticity from the early interaction. The rightward (upstream)

advance of these structures makes it more likely that they are the tip vortex of the test blade. Further clarification of the source of this structure is available from its geometric position. A simple geometric reckoning of the rotor tip path, and its subsequent deformation as it is convected downstream at the tunnel freestream velocity, would indicate that tip flows should be expected to intercept the light sheet at a position 299 mm aft of the aerofoil leading edge at this point in the interaction. The proximity of this predicted intercept position to the position of the vortical flows noted in the present data image therefore reinforces the premise that this structure is indeed the tip vortex.

Discussion

The results from a BVI investigation have been presented. The vortical flows generated during interactions have been captured utilizing PIV. Both the deformation and division of the interaction vortex have been documented. In addition, the blade's own tip vortex and a vortex generated during the trailing-edge interaction have been observed.
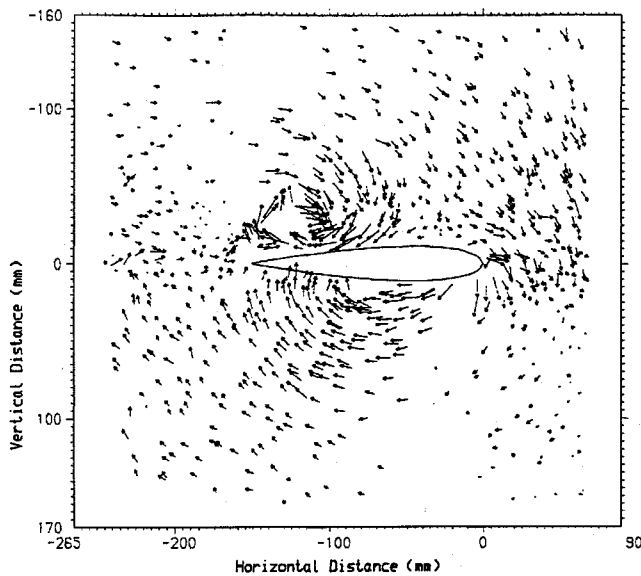
Fig. 5e   PIV data collected during a parallel, head-on, BVI; Γ_c = 3.4 m²/s, r/R = 0.78, Y_v/c = 0.0, and Ψ = 182 deg: →, 10 m/s; →, 20 m/s; and ——→, 30 m/s.

Fig. 5g   PIV data collected during a parallel, head-on, BVI; Γ_c = 3.4 m²/s, r/R = 0.78, Y_v/c = 0.0, and Ψ = 186 deg: →, 10 m/s; →, 20 m/s; and ——→, 30 m/s.

Fig. 5f   PIV data collected during a parallel, head-on, BVI; Γ_c = 3.4 m²/s, r/R = 0.78, Y_v/c = 0.0, and Ψ = 184 deg: →, 10 m/s; →, 20 m/s; and ——→, 30 m/s.
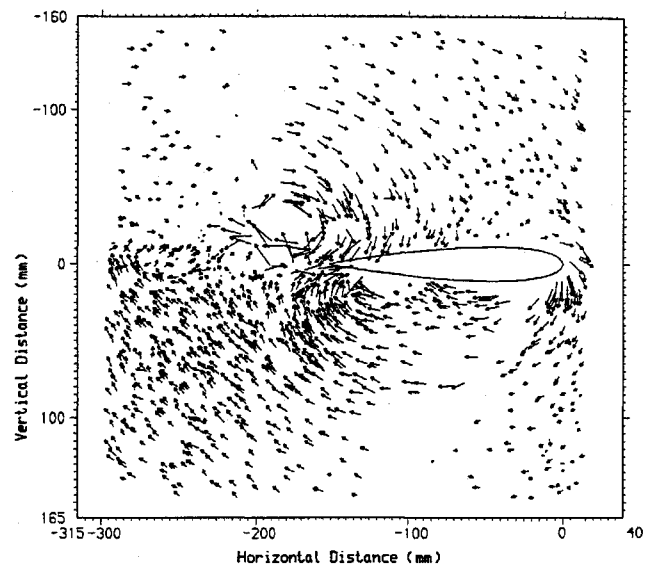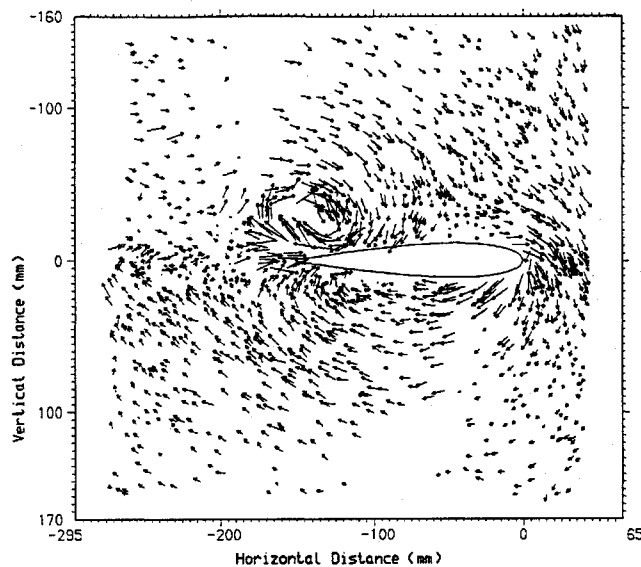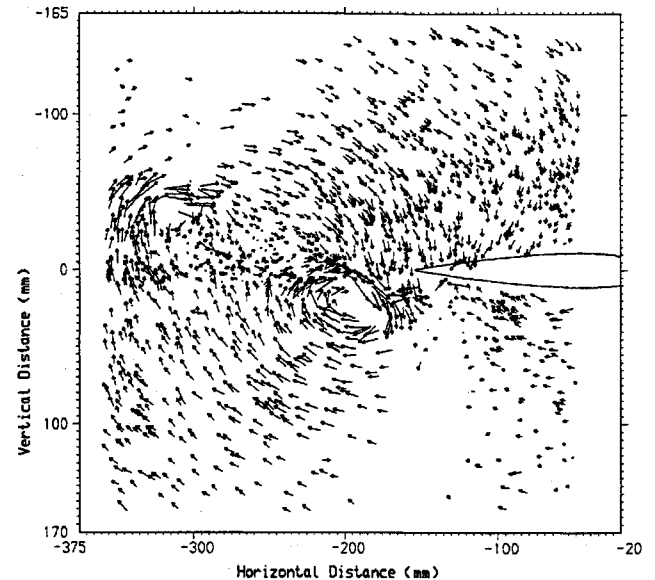

Fig. 5h   PIV data collected during a parallel, head-on, BVI; Γ_c = 3.4 m²/s, r/R = 0.78, Y_v/c = 0.0, and Ψ = 191 deg: →, 10 m/s; →, 20 m/s; and ——→, 30 m/s.

Previous investigations in the University of Glasgow BVI facility[9-21] have utilized pressure instrumentation to provide pressure profiles measured about the rotor blade. Such pressure data were also integrated about the blade chord to document force and moment histories. An example of these is presented in Fig. 6. The upper plot presents normal force data, the middle plot contains quarter-chord moment data, and the lower plot is the tangential force data. The data in these plots were collected under the same conditions as the data of Fig. 5: Y_v/c = 0.0, Z_v/c = 0.0, and Γ_c = 3.4 m²/s, and the data were collected at the 78.5% span location.

Eight timing lines have been added to indicate the position of the corresponding data presented in Fig. 5. The first line, near X_v/c = −0.4, corresponds with the data of Fig. 5a. At this point the blade is entering a region of strong vortex-induced upwash. This increase in leading-edge incidence accelerates flows in front of the blade and above the leading edge, while decelerating flows near the lower surface. This mechanism, by which the large leading-edge incidence produces accelerated flows (and thus large suction peaks) near the leading edge, will be referred to as the incidence effect. This

incidence effect is the underlying cause of the large and growing values in both C_n and C_t evident at the first timing line. The positive C_m values evident at this position also reflect the forward chord station of these velocity effects, and the corresponding forward position of the resulting pressure differential.

The second timing line in Fig. 6, near X_v/c = −0.2, corresponds with the maximum in C_n and very nearly the minimum in C_t. The corresponding PIV image (Fig. 5b) shows that at this point the blade has reached the edge of the vortex core and the greatest upwash induced by the vortex. This increase in upwash results in an increase in all of the effects noted at the first timing line: accelerations in velocities about the leading edge driving up the C_n and C_t values and the forward position of these effects driving up C_m.

By the time the interaction has progressed to the third timing line, the integrated force histories show dramatic reversals, and the moment history shows a slight reversal from the local peak at the previous timing line. The corresponding PIV image (Fig. 5c) reveals that at this point the blade leading edge has penetrated through the core of the vortex, reaching beyond the region of strong vortex-induced
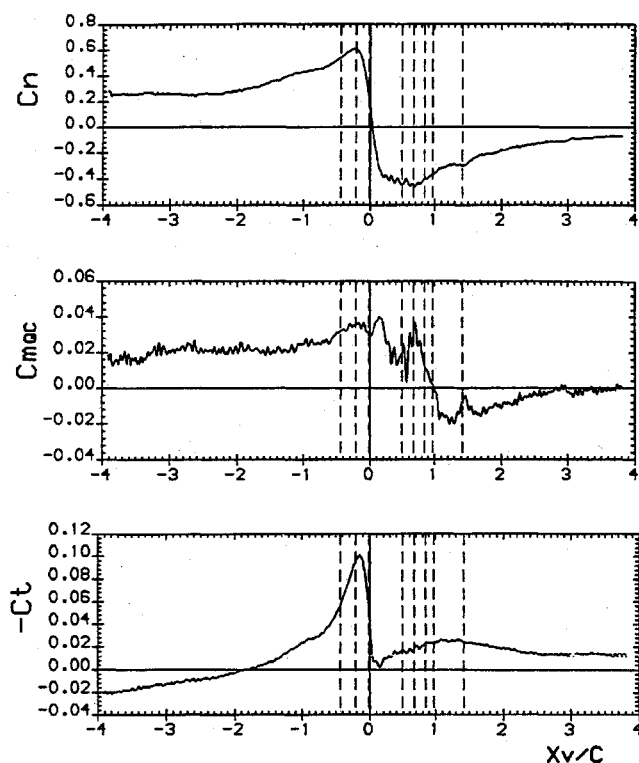
Fig. 6 C_n, C_{mQC}, and C_t data collected during a parallel BVI; $\Gamma_c = 3.4$ m²/s, $r/R = 0.78$, and $Y_v/c = 0.0$. The timing lines indicate the positions of the corresponding PIV images in Fig. 5.

upwash, to a region with only a very weak upwash. The resulting changes to the leading-edge incidence greatly reduce the flow velocities past the leading edge and upper surface, resulting in a decline in all of the integrated coefficients. The decline in moment is partially ameliorated by the lower surface vortex fragment, which enhances nose-up moments through the retardation of local (surface) flow velocities and the resulting enhancement in local pressures. This second mechanism, by which local blade surface pressure is influenced by the proximity of the vortex fragments, has been christened the local suction effect.

By the time of the fourth timing line, near $X_v/c = 0.5$, the integrated force histories have completed their reversal. The corresponding PIV image (Fig. 5d) reveals that the blade leading edge has penetrated past the vortex core (splitting it completely into two fragments) and has passed into regions of vortex-induced downwash. This negative incidence is also manifest in nearly maximum values of negative lift. The moment is also continuing to drop, as the enhanced flows of the upper surface vortex fragment and the retarded flows of the lower surface fragment act together to pull up on further aft positions of the blade chord. Throughout the interaction these local suction effects are most clearly evident in their effect upon C_m. Their effect upon C_n is generally overshadowed by the effect of leading-edge incidence variations. At this point in the interaction C_t remains near zero, as leading-edge suctions (associated with the negative incidence) compete with the local suction produced by the upper vortex fragment near the aft portion of the blade.

The fifth timing line, near $X_v/c = 0.7$, corresponds with the PIV image of Fig. 5e. At this point in the interaction C_n has reached its absolute nadir, C_m approaches a local maximum, and C_t remains near zero. The corresponding PIV image reveals that at this point the incidence remains negative, producing strong negative lift. Furthermore the upper vortex fragment has reached the trailing edge, so that the suctions on the upper surface are about to pass from above the blade, allowing a slight recovery of further negative lift. In addition the small trailing-edge vortex is generated at the trailing edge at this point. This trailing-edge vortex has the opposite sense of the interaction vortex fragments and appears to develop

between the upper vortex fragment and the blade. This further increases upper surface pressures, producing a small amount of further negative lift, but greatly affecting the C_m history by pushing the trailing edge down and producing a strong transient peak in the moment history. The effect of all of these trailing-edge flows upon C_t is minimal, reflecting the weak horizontal force components produced upon these nearly horizontal blade surfaces. Instead the weak leading-edge suctions dominate C_t, preserving the weak forward force evident throughout the later portions of the interaction. The weak clockwise vorticity that is evident in the wake is found inconsistent with the continuously dropping C_n evident for much of the interaction preceding this timing line.

The sixth timing line, near $X_v/c = 0.8$, corresponds with the flows of Fig. 5f. The slight advance since the last timing line has been sufficient to allow the trailing-edge vortex (underlying the moment spike at the previous timing line) to convect past the trailing edge. This results in the loss of that (small) portion of negative C_n attributable to the higher pressures produced by the flow retardation effected by this vortex. More importantly, the trailing-edge passage of this vortex results in the sharp drop in C_m from the spike evident at the previous timing line. Again the effect of the trailing-edge passage of the vortex fragments is seen to have little effect upon the C_t history. Throughout this interaction the only time that any substantial counterclockwise vorticity is seen entering the wake is during the trailing-edge interaction. Given the present (weak) increase in C_n, shed vorticity of this sense of rotation is not expected. This continued mismatch of wake vorticity and blade circulation changes suggests that there is a lag between blade circulation changes and the appearance of the shed vorticity entering the wake. This would imply that the present near wake shear is the belated result of the large C_n collapse.

By the seventh timing line, near $X_v/c = 1.0$, the entire upper surface vortex fragment has passed into the wake (see Fig. 5g). This has little effect upon the development of the force and moment histories, presumably because the effect of this fragment upon surface flows was already greatly compromised by the presence of the trailing-edge vortex. The term C_n remains negative but begins to converge back towards zero as the negative incidence fades. The moment continues to drop away from the moment spike produced by the trailing-edge vortex. This drop is further aided by the lower vortex fragment, and its associated flow retardations, as they approach the trailing edge and push up on more aft sections of the blade chord. These extra trailing-edge pressures may also underlie the continued development of the forward force, despite the gradual fading of leading-edge incidence.

The final timing line, near $X_v/c = 1.4$, corresponds with the PIV image of Fig. 5h. This image captures the lower vortex fragment passing the trailing edge and possibly followed by another counterclockwise trailing-edge vortex. This lower surface vortical structure is similar to that generated under similar conditions during lower surface BVIs (see Refs. 20 and 21). Although the PIV image is not clear in the presentation of this second trailing-edge vortex, the orientation of many of the velocity vectors near the trailing edge are consistent with its presence. The effect of such a vortex would also be consistent with the perturbations seen in the C_n and C_m histories. The local dip in C_n and the local peak in C_m would both be consistent with a little extra suction beneath the trailing edge. This brief surge of suction would be consistent with the enhanced surface velocities produced by the counterclockwise rotation of this vortex. As at the previous several timing lines, these events at the trailing edge appear to have little effect upon the C_t history.

Conclusions

The results of a PIV study have been presented. The velocity field observed during these tests was dominated by the vortical flows of the main interaction vortex. During head-on interactions the blade was found to split the interaction vortex into two fragments. The lower fragment was seen to distort and spread across the lower aerofoil surface, whereas the upper fragment was only slightly distorted. Secondary vortices were found to form on both surfaces as the vortex passed the trailing edge. Both of these secondary vortices were found to contribute to further vortex deformation as the main interaction vortex entered the wake.

The PIV data collected during head-on BVIs were found to correspond well with the pressure data collected in earlier investigations. The aerodynamic response of the test blade was driven by the interaction vortex through two mechanisms: 1) the effect of the interaction vortex upon the effective incidence of the blade and 2) the effect of the interaction vortex upon flows near the blade surface as the interaction vortex (or its fragments) convected past.

The first of these mechanisms was found to dominate the normal force and tangential force histories through the production of a large leading-edge suction peak. The second mechanism had a lesser effect upon normal and tangential forces but dominated the quarter-chord moment history. In addition, the secondary vortices generated during the trailing-edge interaction were found to affect the integrated force and moment histories through the alteration of local surface velocities near the trailing edge.

Acknowledgments

References

[1]Scheiman, J., and Ludi, L. H., "Qualitative Evaluation of Effect of Helicopter Rotor-Blade Tip Vortex on Blade Airloads," NASA TN D-1637, May 1963.

[2]Brotherhood, P., and Riley, M. J., "Flight Experiments on Aerodynamic Features Affecting Helicopter Blade Design," Vertica, Vol. 2, No. 1, 1978, pp. 27–42.

[3]Schmitz, F. H., Boxwell, D. A., Lewy, S., and Dahan, C., "Model-to Full-Scale Comparisons of Helicopter Blade-Vortex Interaction Noise," Proceedings of 38th Annual National Forum of the American Helicopter Society (Anaheim, CA), American Helicopter Society, Washington, DC, 1978.

[4]Surendraiah, M., "An Experimental Study of Rotor Blade-Vortex Interaction," M.S. Thesis, Dept. of Aerospace Engineering, Pennsylvania State Univ., University Park, PA, Dec. 1969.

[5]Padakannaya, R., "Experimental Study of Rotor Unsteady Airloads Due to Blade Vortex Interaction," NASA CR-1909, Nov. 1971.

[6]Caradonna, F. X., Laub, G. H., and Tung, C., "An Experimental Study of Rotor-Vortex Interaction," NASA TM-86005, Nov. 1984.

[7]Caradonna, F. X., Lautenschlager, J. L., and Silva, M. J., "An Experimental Study of Rotor-Vortex Interactions," AIAA Paper 88-0045, Jan. 1988.

[8]Caradonna, F. X., Strawn, R. C., and Bridgeman, J. O., "An Experimental and Computational Study of Rotor-Vortex Interactions," Proceedings of 14th European Rotorcraft and Powered Lit Aircraft Forum (Milan, Italy), Associazione Italiana di Aeronautica ed Astronautica, Rome, Italy, 1988, pp. 18.1–18.16.

[9]Kokkalis, A., and Galbraith, R. A. McD., "Description of, and Preliminary Results from, a New Blade-Vortex Interaction Test Facility," Proceedings of 12th European Rotorcraft and Powered Lift Aircraft Forum (Garmisch-Partenkirchen, Federal Republic of Germany), 1986, pp. 80.1–80.17.

[10]Kokkalis, A., and Galbraith, R. A. McD., "Results from the Glasgow University Blade-Vortex Interaction Facility," Proceedings of 13th European Rotorcraft and Powered Lift Aircraft Forum (Arles, France), Association Aeronautique et Astronautique de France, 1987, pp. 218-1–218.16.

[11]Saliveros, E., and Galbraith, R. A. McD., "Collected Data from Blade Vortex Interaction Tests Using a Single Blade, Non-Lifting Rotor, Vol. I: 94% Span," Glasgow Univ., G.U. Aero Rept. 9007, Glasgow, Scotland, UK, March 1990.

[12]Saliveros, E., and Galbraith, R. A. McD., "Collected Data from Blade Vortex Interaction Tests Using a Single Blade, Non-Lifting Rotor; Vol. II: 86% Span," Glasgow Univ., G.U. Aero Rept. 9008, Glasgow, Scotland, UK, March 1990.

[13]Saliveros, E., and Galbraith, R. A. McD., "Collected Data from Blade Vortex Interaction Tests Using a Single Blade, Non-Lifting Rotor; Vol. III:

[14]Saliveros, E., and Galbraith, R. A. McD., "Collected Data from Blade Vortex Interaction Tests Using a Single Blade, Non-Lifting Rotor, Vol. IV: 70% Span," Glasgow Univ., G.U. Aero Rept. 9010, Glasgow, Scotland, UK, March 1990.

[15]Saliveros, E., and Galbraith, R. A. McD., "Collected Data from Blade Vortex Interaction Tests Using a Single Blade, Non-Lifting Rotor; Vol. V: 62% Span," Glasgow Univ., G.U. Aero Rept. 9011, Glasgow, Scotland, UK, March 1990.

[16]Horner, M. B., Saliveros, E., Kokkalis, A., and Galbraith, R. A. McD., "Results from a Set of Low Speed Blade-Vortex Interaction Experiments," Journal of Experiments in Fluids, Vol. 14, May 1993, pp. 341–352.

[17]Horner, M. B., Saliveros, E., and Galbraith, R. A. McD., "An Experimental Investigation of the Oblique Blade-Vortex Interaction," Aeronautical Journal, Vol. 96, No. 955, 1992, pp. 184–191.

[18]Horner, M. B., Saliveros, E., and Galbraith, R. A. McD., "An Examination of Vortex Convection Effects During Blade-Vortex Interaction," Aeronautical Journal, Vol. 96, No. 960, 1992, pp. 373–379.

[19]Horner, M. B., and Galbraith, R. A. McD., "An Examination of the Effects of Blade-Vortex Interaction on Flows Near the Blade Tip," Proceedings of 18th European Rotorcraft and Powered Lift Aircraft Forum (Avignon, France), Association Aeronautique et Astronautique de France, 1992, pp. 136-1–136-12.

[20]Horner, M. B., Stewart, N., Galbraith, R. A. McD., Grant, I., Coton, F. N., and Smith, G. H., "Preliminary Results from a Particle Image Velocimetry Study of Blade-Vortex Interaction," Proceedings of 19th European Rotorcraft and Powered Lift Aircraft Forum (Cernobbio, Italy), Associazione Italiana di Aeronautica ed Astronautica, Rome, Italy, 1993, p. C3-1–C3-18.

[21]Horner, M. B., "An Examination of Blade-Vortex Interaction Utilising Pressure Measurements and Particle Image Velocimetry," Ph.D. Dissertation, Dept. of Aerospace Engineering, Univ. of Colorado, Boulder, CO, May 1994.

[22]Seath, D. D., "Vortex-Airfoil Interaction Tests," Proceedings of 2nd Atmospheric Flight Mechanics Conference (Palo Alto and Moffett Field, CA), AIAA, 1972.

[23]Seath, D. D., Kim, J. M., and Wilson, D. R., "An Investigation of the Parallel Blade-Vortex Interaction in Low-Speed Wind Tunnel," AIAA Paper 87-1345, June 1987.

[24]Ham, N. D., "Some Preliminary Results from an Investigation of Blade-Vortex Interactions," Journal of the American Helicopter Society, Vol. 19, No. 2, 1974, pp. 45–48.

[25]Ham, N. D., "Some Conclusions from an Investigation on Blade-Vortex Interaction," Journal of the American Helicopter Society, Vol. 20, Oct. 1975, pp. 26–31.

[26]Booth, E. R., Jr., and Yu, J. C., "Two-Dimensional Blade-Vortex Flow Visualisation Investigation," AIAA Journal, Vol. 24, No. 9, 1986, pp. 1468–1473.

[27]Booth, E. R., Jr., "Surface Pressure Measurement During Low Speed Two-Dimensional Blade Vortex Interaction," AIAA Paper 86-1856, July 1986.

[28]Meier, G. E. A., and Timm, R., "Unsteady Vortex Airfoil Interaction," AGARD CP-386, May 1985.

[29]Straus, J., Renzoni, O., and Mayle, R. E., "Airfoil Pressure Measurements During a Blade-Vortex Interaction and a Comparison with Theory," AIAA Paper 88-0669, Jan. 1988.

[30]Huyer, S. A., and Luttges, M. W., "Unsteady Flow Interactions Between the Wake of an Oscillating Airfoil and a Stationary Trailing Airfoil," AIAA Paper 88-2581, June 1988.

[31]Ziada, S., and Rockwell, D., "Vortex-Leading Edge Interaction," Journal of Fluid Mechanics, Vol. 118, May 1982, pp. 79–107.

[32]Walker, J., "Dynamic Stall Wake Interaction with a Trailing Aerofoil," AIAA Paper 87-0239, Jan. 1987.

[33]Sears, W. R., "Aerodynamics, Noise and the Sonic Boom," AIAA Journal, Vol. 7, No. 4, 1969, pp. 577–586.

[34]Panaras, A., "Numerical Modelling of the Vortex-Airfoil Interaction," AIAA Journal, Vol. 25, No. 1, 1987, pp. 5–11.

[35]Lee, D. J., and Smith, C. A., "Distortion of Vortex Core During Blade/Vortex Interaction," AIAA Paper 87-1243, June 1987.

[36]Jones, H. E., and Caradonna, F. X., "Full Potential Modelling of Blade-Vortex Interactions," Vertica, Vol. 12, No. 1/2, 1988, pp. 129–145.

[37]Liu, A., "The Development of Image Processing Techniques and Their Applications in Particle Image Velocimetry," Ph.D. Dissertation, Dept. of Civil and Offshore Engineering, Heriot-Watt Univ., Edinburgh, Scotland, UK, May 1990.